Research Square

Preprints are preliminary reports that have not undergone peer review.
They should not be considered conclusive, used to inform clinical practice,
or referenced by the media as validated information.

Rapid transient uplift driven by active slab tear: southern Calabria, Italy

Rebecca Dorsey

rdorsey@uoregon.edu

University of Oregon

Nathan Brown

University of Texas at Arlington https://orcid.org/0000-0002-7385-8679

Sergio Longhitano

Università della Basilicata

Marco Meschis

Istituto Nazionale di Geofisica e Vulcanologia (INGV), Sezione Palermo

Domenico Chiarella

University of Bologna https://orcid.org/0000-0003-2482-0081

Charles Ogle

Department of Earth Sciences, University of Oregon

Article

Keywords:

Posted Date: August 6th, 2026

DOI: https://doi.org/10.21203/rs.3.rs-10297103/v2

License: This work is licensed under a Creative Commons Attribution 4.0 International License.
Read Full License

Additional Declarations: There is **NO** Competing Interest.

Version of Record: A version of this preprint was published at Communications Earth & Environment on November 6th, 2026. See the published version at https://doi.org/10.1038/s43247-026-04207-2.

Rapid transient uplift driven by active slab tear: southern Calabria, Italy

Authors: Rebecca J. Dorsey[1*], Nathan D. Brown[2], Sergio G. Longhitano[3], Marco Meschis[4], Domenico Chiarella[5], Charles P. Ogle[1]

Affiliations
[1]Department of Earth Sciences, University of Oregon, Eugene, OR, 97403
[2]Department of Earth and Environmental Sciences, University of Texas at Arlington, Arlington, TX, USA
[3]Department of Basic and Applied Sciences, Università degli Studi della Basilicata, Potenza, Italy
[4]Istituto Nazionale di Geofisica e Vulcanologia (INGV), Sezione Palermo, Palermo, Italy
[5]Department of Biological, Geological and Environmental Sciences, University of Bologna, Bologna, Italy

*Correspondence to: rdorsey@uoregon.edu

Abstract

Southern Italy preserves a well-studied record of deformation and uplift related to migrating oblique collision, trench retreat, and tearing of subducted ocean slabs. However, the surface expression of these processes is incompletely understood due to a lack of reliable ages for marine terraces >200 m above sea level (masl). Here we use luminescence methods to date shallow marine sands from terraces ~ 100 to 1,000 masl in southern Calabria and interpolate the results with regional surface mapping. Burial ages overlap across the full range of sampled elevations with a weighted mean of 118.8 ± 8.7 thousand years before present (ka). These ages, combined with map data and fault-zone morphology, indicate that the terraces are erosional remnants of a single, once-continuous deformed surface. Calculated uplift rates vary from <1 to >12 mm yr^{-1} and throw rates on active normal faults are 0.8–4.2 mm yr^{-1}. We infer that rapid post-120 ka uplift is an ongoing isostatic response to an active tear in the Ionian slab, consistent with recent geophysical observations and predictions of geodynamic models. These results have important implications for assessment of geohazards in southern Calabria and northeast Sicily, one of the highest seismic risk areas in the Mediterranean region.

Introduction

Uplift and subsidence of the Earth's surface occurs in response to crustal deformation (i.e., thickening or thinning) and mantle processes such as rising plumes, circulation above subduction zones, and dynamic effects associated with slab breakoff[1–3]. While crustal and mantle drivers of vertical motions are both commonly active at convergent and strike-slip margins, it is difficult to discern their relative contributions to construction of topography[4]. Crustal thickness and density data can be used to isolate the component of topography supported by the mantle[3], but this approach cannot detect changes in time. Geologic histories of orogenic uplift and exhumation are revealed by inversion of thermochronology and geomorphic datasets[5], without the temporal resolution needed to detect changes in rate over shorter timescales (10^4-10^5 yr). Dating of marine terraces is commonly used to determine late Pleistocene uplift rates[6–8], but the results often are not diagnostic of a unique mechanism. Thus, we currently are limited in our ability to distinguish crustal versus mantle drivers of surface uplift in tectonically active settings.

Southern Italy (Fig. 1a) is well suited for new studies to address this knowledge gap. The Apennine Mountains formed by thrusting of Mesozoic paleo-Tethys Ocean rocks over the Adriatic microplate during Cenozoic collision between Africa and Europe, while the Tyrrhenian Sea opened by extension due to rapid rollback and southeastward retreat of the Ionian subduction zone[9,10]. Progressive tearing and breakoff of the composite Adriatic-Ionian slab[11–13] produced a southeast-migrating wave of Pliocene-Pleistocene uplift along the central to southern Apennine thrust belt and adjacent wedge-top basins[14,15]. Tomographic data suggest slab tearing is complete beneath the southern Apennines, northern Calabria, and northeast Sicily, and that a ~100-km segment of the Ionian slab is still intact (undetached) beneath southern Calabria[5,13,16–18]. However, some studies find evidence for a small or incipient slab tear along this segment[19–22] and suggest an active tear is propagating south beneath the Serre Mountains[23]. Early studies of slab tearing in Italy were inconclusive on this question and cautioned that the resolution of tomographic models is insufficient to determine if the Ionian slab is intact or torn in southern Calabria[11,12].

This uncertainty can be addressed with new data to constrain rates and timescales of surface uplift. Two hypotheses, uncoupling along a weak subduction fault and thickening of forearc crust by underplating, are unlikely because they predict uplift rates and timescales that are incompatible with the known tectonic evolution of Calabria[17]. Two other hypotheses that invoke mantle processes – toroidal flow of upper mantle around the torn edges of a retreating slab[3,17], and unloading due to slab breakoff[11,12,24] – can be tested through dating of marine terraces to determine uplift rates. The toroidal flow hypothesis predicts uplift at rates of 1-2 mm yr^{-1} over ~1 Myr[5,17], whereas isostatic rebound due to slab breakoff predicts much faster rates (5–14 mm yr^{-1}) for a shorter time (<500 kyr)[25,26]. These predictions specify terrace ages and elevations that should be observed if the underlying assumptions are correct, allowing us to test models for the primary mechanism of uplift in this setting.

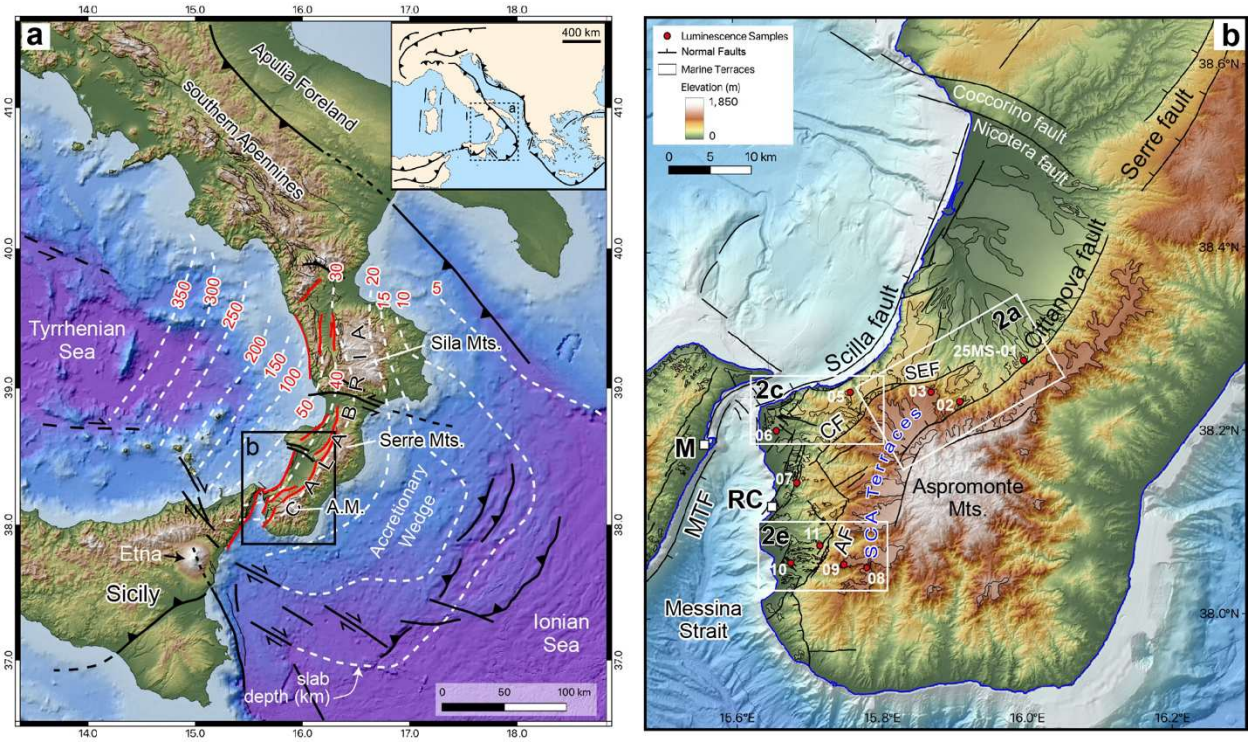


Figure 1. (a) Tectonic setting of southern Italy. Dashed white lines are depth to top of the subducting Ionian slab (refs. 19, 21). Red lines are major active normal faults in Calabria and NE Sicily; black lines are thrust and strike-slip faults. A.M. is Aspromonte Mts. (b) Digital elevation model (DEM) of southern Calabria showing Pleistocene marine terraces, active normal faults, luminescence sample locations, and location of detailed maps in Figure 2. AF, Armo fault; CF, Calanna fault; M, Messina; MTF, Messina-Taormina fault; RC, Reggio Calabria; SEF, Sant'Eufemia fault.

Late Cenozoic extension in southern Calabria and NE Sicily has produced a network of seismically active normal faults that bound the Messina Strait (Fig. 1) and generate frequent damaging earthquakes[27–33]. The faults offset Pleistocene marine terraces whose ages were originally estimated with paleontological evidence and shoreline modeling[24,34,35]. These studies concluded that marine terraces higher than ~1,000 m above sea level (masl) are ca. 1.0-1.2 Ma, and this age has been used to calculate uplift and fault-throw rates[28–30]. The original terrace chronologies are supported with newer luminescence and ^{14}C ages at elevations <200 masl[36,37], but no direct age constraints exist for terraces higher than ~200 masl. A recent study found that the high-elevation terraces are all younger than 0.48 Ma[38], raising new questions about the timing, rates, and drivers of uplift in this region.

Here we integrate luminescence dating of marine terraces with surface mapping and fault-zone morphology to test hypotheses for the current state of the Ionian slab beneath southern Calabria. This approach allows us to quantify magnitudes and rates of Pleistocene uplift, erosion, and fault throw, providing new insight into the role of mantle processes on crustal extension and landscape evolution. The data reveal rapid production of mountainous topography over the past ~120 kyr that is best explained by active tearing of the subducted Ionian slab. We thus document a rare example of modern transient response to strong mantle-surface coupling via slab tear that is widely applicable to other subduction systems.

Results

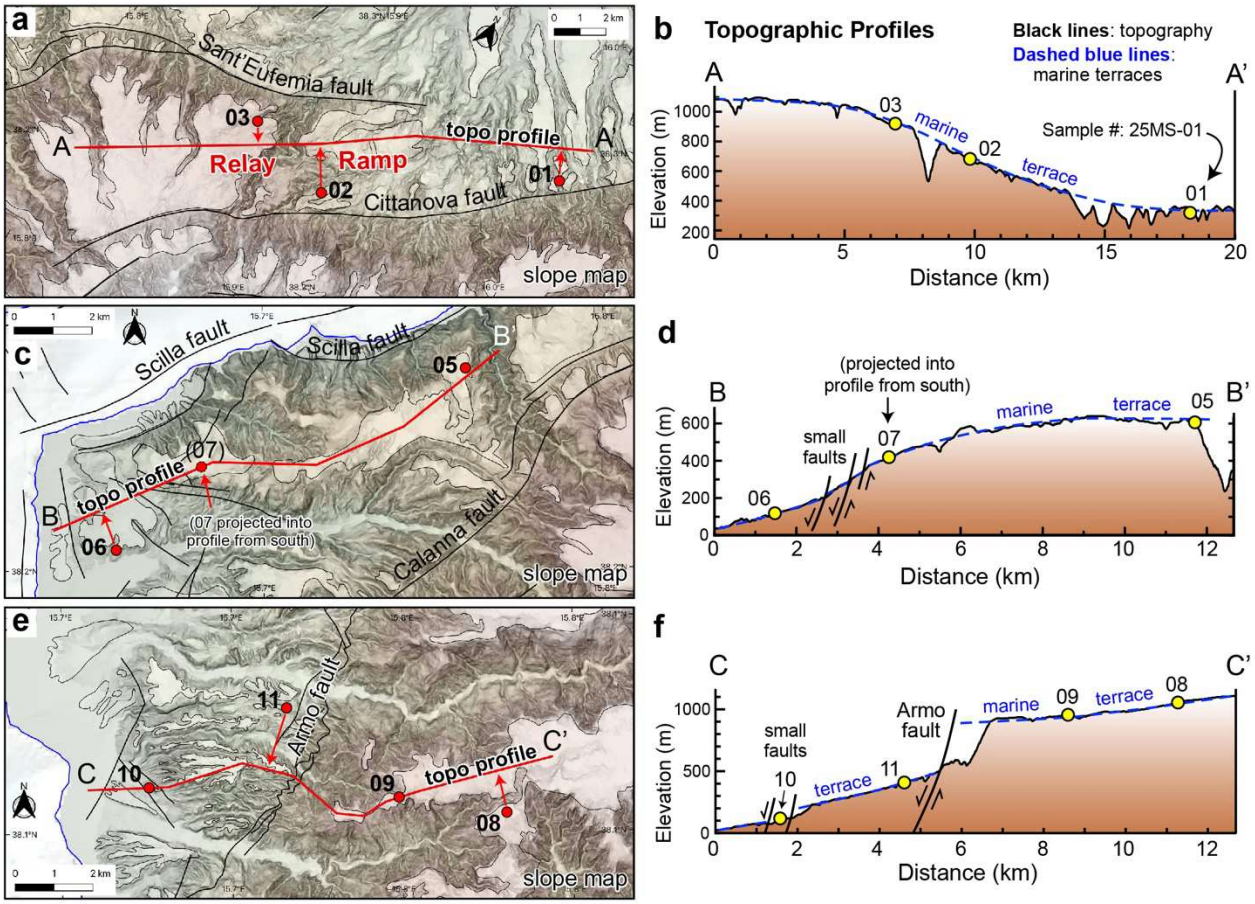
Marine terraces and fault-zone morphology

Marine terraces in southern Calabria are offset and uplifted within a complex network of seismically active normal faults (Fig. 1b). The terraces can be correlated across a wide range of elevations using geologic maps, cross sections, regional stratigraphy, fossil content, sedimentology, cement characteristics, and diagnostic morphology of a large relay ramp[38]. A belt of large, low-relief high-elevation terraces known as the “SCA terraces” (for the Serre, Cittanova and Armo faults that cut them)[29] is preserved between ~ 900 and 1,200 m elevation in the hanging wall of the Cittanova fault and footwall of the Armo and Sant’Eufemia faults (Fig. 1b). Terrace margins are truncated at their edges by deep canyons incised up to ~500 m

into older Cenozoic strata and pre-Cenozoic crystalline bedrock. Sedimentary facies include well-sorted beach sands, fossiliferous shallow marine sands, molluscan shell beds, bioherms, stratified delta gravels, minor fluvial red beds, and matrix-rich gravels locally preserved near active faults (ref. [38]; this study).

The topography of the study area can be divided into three main elevation belts (Fig. 1b): (i) a low-elevation coastal belt ≤200 masl; (ii) a zone of uplifted, faulted, and incised marine terraces between ~200 and 1,300 masl; and (iii) the high Aspromonte Mountains ~1,300 –1,850 masl in the footwall of the highest-elevation normal faults. Major incised trunk canyons of zone (ii) are arranged in a quasi-radial pattern that originates in the core of the high Aspromonte Mountains. Local relief increases stepwise across active normal faults, and bedrock channels are incised up to 500 m below the eroded base of marine terraces in the footwall of the Armo and Sant'Eufemia-Calanna faults (see also refs. [29,30]).

Marine terraces form low-relief, gently inclined geomorphic surfaces that dip ~1°–4° with dip directions parallel and perpendicular to the strike of normal faults that cut them (Fig. 2). Hanging-wall tilt ramps dip away from adjacent footwall blocks, unlike most extensional systems where hanging-wall dip slopes tilt toward the adjacent footwall. North of the Aspromonte Mountains, a widespread unit of fossiliferous beach sands climbs gradually up a relay ramp from ~350 to 1,050 masl between the Cittanova and Sant'Eufemia faults[27,38] (Figs. 2a, 2b). West of there, terrace deposits in the footwall of the Scilla fault descend from 600 to 100 masl due to an along-strike decrease in throw toward the tip of the fault where extensional strain is transferred across the Messina Strait to opposite-dipping faults in NE Sicily (Figs. 2c, 2d)[33]. A southern transect reveals ca. 400 m of throw on the Armo fault and an inclined ramp in the hanging wall that dips ~5° away from the fault (Figs. 2e, 2f). An oblique view of topography (Fig. 3a) reveals the 3-dimensional architecture of this dynamic landscape sculpted by deep incision associated with uplift on active normal faults.



135

136 Figure 2. Geomorphic and structural setting of luminescence samples dated in this study. (a, c, e)
137 Slope maps with marine terraces (outlined), active normal faults (black lines), sample locations, and
138 topographic profile lines. (b, d, f) Topographic profiles showing deformed marine terraces, sample
139 positions, and faults.

140

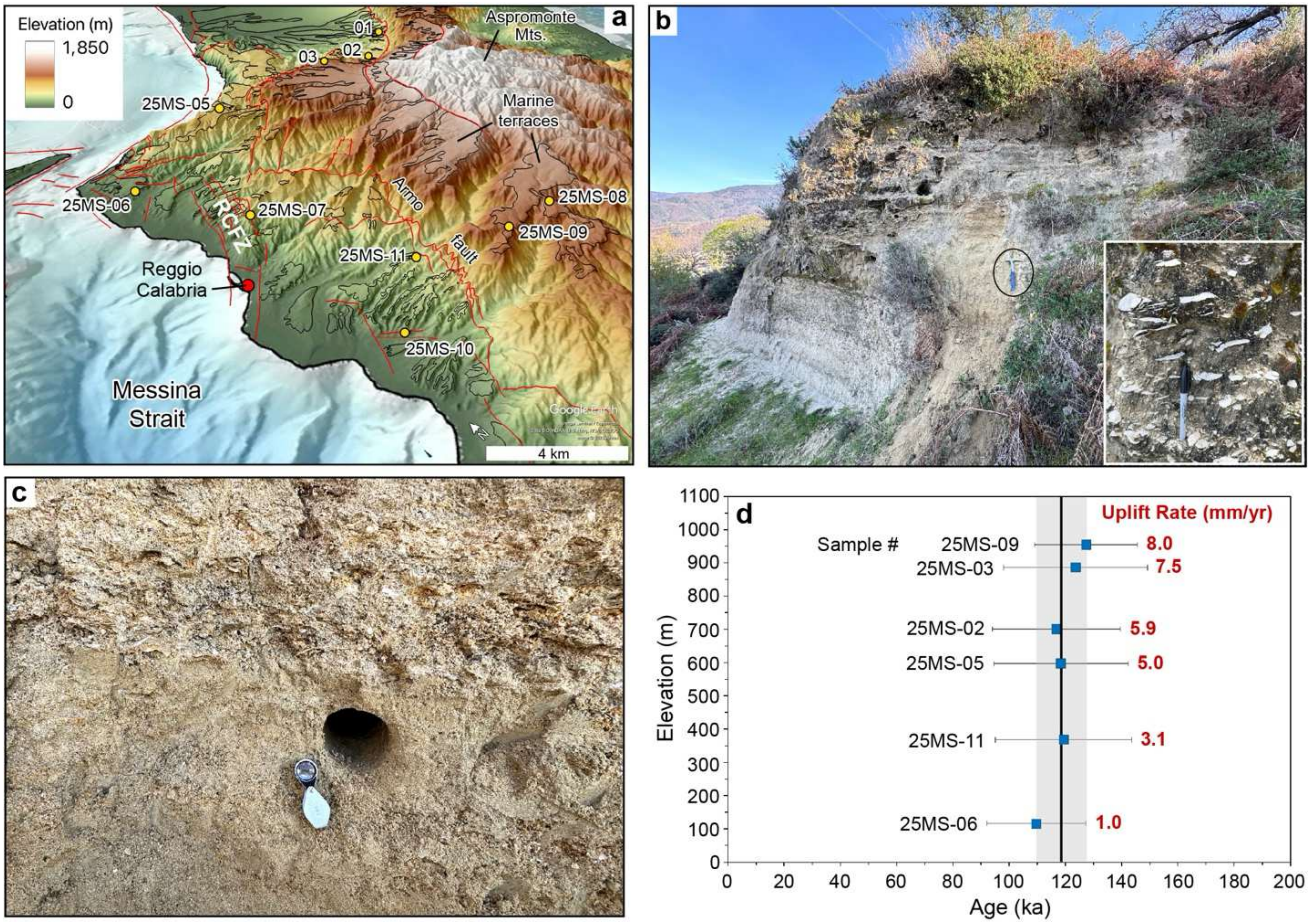


Figure 3. (a) Oblique view of color DEM on shaded-relief topography showing sample sites (numbered), marine terraces (outlined), and active normal faults (red lines). RCFZ: Reggio Calabria fault zone. (b) Sample site 25MS-02 in cross-bedded shallow marine sands with shell concentrations (inset; sharpie pen is 13.5 cm long). Hammer (circled) is 32.5 cm long. (c) Sample site 25MS-09 in shallow marine shelly sand; hand lens is 5.5 cm long. (d) Fading-corrected luminescence ages of terrace sands (Supplementary Tables 1, 2). The weighted mean age is 118.8 ± 8.7 ka (vertical line and gray box; ± 1 sigma). Uplift rates are calculated from the mean age (118.8 ka) and sample elevations.

Constraining uplift and fault-throw rates

Samples of weakly cemented sand were collected for luminescence dating from marine terraces at elevations 107 to 1040 masl (Figs. 2, 3b, 3c; Supplementary Table 1). Luminescence ages record the time since sediment grains were last exposed to sunlight. To estimate the burial ages of the collected sediments, we used a single-grain post-infrared infrared stimulated luminescence measurement protocol applied to sand-sized K-feldspar grains (see Methods for full description). This technique resolves the full distribution of

157 apparent ages within a deposit and is well suited for depositional contexts where not every
158 grain was sufficiently exposed to sunlight prior to burial. Three hundred grains were
159 stimulated per sample, from which the number of accepted grains ranged from 65 to 197
160 (Supplementary Table 2). For all samples, the single-grain equivalent dose values were more
161 variable than would be expected for a single dose population, with overdispersion values of
162 about 40-60%. We therefore used the minimum dose model to summarize the equivalent
163 dose of each sample (Supplementary Figs. 1–3). These samples required a modest fading
164 correction (*g*-value of 0.855 ± 0.135 % loss per decade) (Supplementary Fig. 4), after which
165 6 of the 10 analysed samples gave apparent ages resolvably below field saturation.
166 Luminescence burial ages all overlap at 1σ error across the full range of sampled
167 elevations (Supplementary Table 2) with a weighted mean of 118.8 ± 8.7 ka (Fig. 3d). The
168 similar age of terraces at different elevations is consistent with – and predicted by – physical
169 evidence for correlation of terrace sediments that originally formed a continuous low-relief
170 depositional surface[38]. Time-averaged uplift rates based on the mean terrace age and
171 sample elevations vary from 1.0 to 8.0 mm yr^{-1} (Fig. 3d), reflecting variations in structural
172 position and elevation of samples collected from a regional unit with the same depositional
173 age (Figs. 1b, 2). Using a mean terrace age of 118.8 ka and lateral continuity of terraces
174 revealed by detailed surface mapping, we interpolate the results to quantify the distribution
175 of uplift rates in the study area (Fig. 4). Rates change abruptly across active normal faults
176 and gradually along inclined structural ramps, varying from <1 mm yr^{-1} near the coast to >12
177 mm yr^{-1} at the highest terrace elevations. The distribution of uplift rates in Fig. 4 is consistent
178 with values determined in a recent comparison of geologic and geodetic vertical rates in
179 Calabria (geologic control sites <200 masl)[39]. Consideration of normal fault kinematics
180 suggests that Pleistocene crustal uplift in the Aspromonte Mountains, in the footwall of the
181 highest-elevation normal faults, likely is faster than the maximum rate of ca. 12 mm yr^{-1}
182 recorded in preserved terraces (Fig. 4). The distribution of small terrace remnants around the
183 flanks of the Aspromonte Mountains suggests a domal uplift geometry in that area.

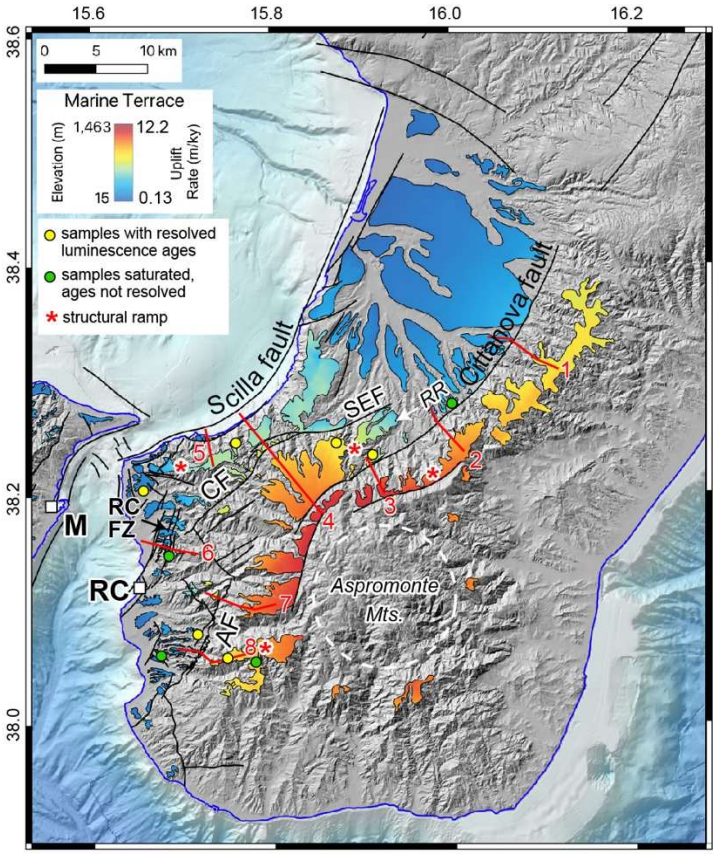


Figure 4. Hillshade topography with marine terraces colored by elevation and calculated uplift rates based on an average age of 119 ka (Fig. 3d) and mapping of correlative terrace surfaces. Uplift rates change abruptly across active normal faults (black lines) and gradually along inclined structural ramps, changing from <1 mm yr-1 near the coast to >12 mm yr-1 at the highest elevations. Numbered red lines are topographic profiles used to estimate throw rate on active normal faults (Table 1). The distribution of isolated terrace remnants around the flanks of the Aspromonte Mountains suggests a domal uplift geometry in that area (dashed white line). AF, Armo fault; CF, Calanna fault; RCFZ, Reggio Calabria fault zone; RR, relay ramp; SEF, Sant'Eufemia fault.

Time-averaged throw rates on major normal faults vary from 0.8 to 4.2 mm yr^{-1} (Table 1; Supplementary Fig. 5). Throw on the Cittanova fault increases from 3.5 ± 0.4 mm yr^{-1} near the tips of the fault to 4.0 ± 0.5 mm yr^{-1} at the center, consistent with common displacement-length profiles on normal faults. Modern ground motions derived from InSAR data show a strong gradient in vertical rate across the Cittanova fault (Supplementary Fig. 6), with a difference of ~3.0–4.5 mm yr^{-1} between hanging-wall and footwall points that overlaps long-term throw rates. The Scilla fault has the largest throw (500 m) and throw rate (4.2 ± 0.5 mm yr^{-1}) observed in this study. A throw of 420 m in the central Armo fault is likely a maximum for this fault and less than 600-700 m estimated in previous studies[29,40]. This

difference reflects our finding that gentle dips on structural ramps should be projected across eroded spans to obtain accurate fault-throw measurements. Despite the smaller offset, our throw rate of 3.5 mm yr^{-1} for the central Armo fault is faster than previous estimates (0.7 mm yr^{-1})[29,40] because the newly obtained age for the offset marine terrace (118.8 ± 8.7 ka) is considerably younger than previous estimates of ~1.0 Ma[24,34,35].

Table 1. Throw rates for major normal faults in the study area (referenced to profiles in Fig. 4)

Profile #	Fault Name	FW elev (m)	HW elev (m)	Throw (m)	Throw Rate (mm yr^{-1})
1	Cittanova fault	840	425	415	**3.5 ± 0.4**
2	Cittanova fault	1000	520	480	**4.0 ± 0.5**
3	Cittanova fault	1200	780	420	**3.5 ± 0.4**
4a	Cittanova fault	1300	1200	100	**0.8 ± 0.1**
4b	Sant'Eufemia–Calanna	1000	610	390	**3.3 ± 0.4**
4c	Scilla fault	520	20	500	**4.2 ± 0.5**
5a	Scilla fault	640	175	465	**3.9 ± 0.5**
5b	Scilla fault	120	20	100	**0.8 ± 0.1**
6a	Reggio Calabria F.Z.	540	210	330	**2.8 ± 0.3**
6b	Reggio Calabria F.Z.	165	60	105	**0.9 ± 0.1**
7	Armo fault (N)	1100	760	340	**2.9 ± 0.4**
8	Armo fault (S)	910	490	420	**3.5 ± 0.4**

- Fault throw = footwall terrace elevation (FW elev) minus hanging-wall terrace elevation (HW elev).
- Terrace elevation is determined by projecting dip on gently inclined structural ramps across an eroded span to the fault (see Extended Data Fig. 5).
- Throw rate = fault throw divided by mean terrace age (118.8 ka).
- Error includes age error (± 8.7 ka) and uncertainty in throw measurement (± 5 %).

Discussion

Surface uplift driven by active slab tear

Drivers of uplift in southern Calabria can be evaluated using data presented above. Toroidal flow of upper mantle around the edges of a torn slab predicts uplift rates of 1–2 mm yr^{-1} in ~1 Myr[5,17], whereas isostatic rebound due to slab tear predicts much faster rates (5–14 mm yr^{-1}) over shorter timescales[25,26]. The slab tear hypothesis is clearly supported by uplift rates of 3–12 mm yr^{-1} since ~120 ka (Figs. 3d, 4). We infer that very rapid post-120 ka uplift is an ongoing isostatic response to a young active tear in the Ionian slab (Fig. 5), consistent with recent geophysical studies that show evidence for a tear in the Ionian slab beneath southern

Calabria[19–22]. High-resolution seismic data reveal a break in hypocenter locations at ~100 km depth[21] that we interpret as a relatively small tear. If the Ionian slab were intact, the attached weight of dense ocean lithosphere would produce slow or moderate surface uplift rates. Isostatic rebound due to an active slab tear is the most likely mechanism appropriate for this tectonic setting that can generate the very rapid short-term uplift rates documented in this study. Slab tear also predicts a short, ~0.5 Myr period of anomalous subsidence immediately prior to basin inversion and switch to rapid uplift[15,26,41], consistent with a known phase of rapid subsidence that produced a regional unit of bathyal marine claystone and marl in southern Calabria between ~ 1.0 and 0.5 Ma[27,38].

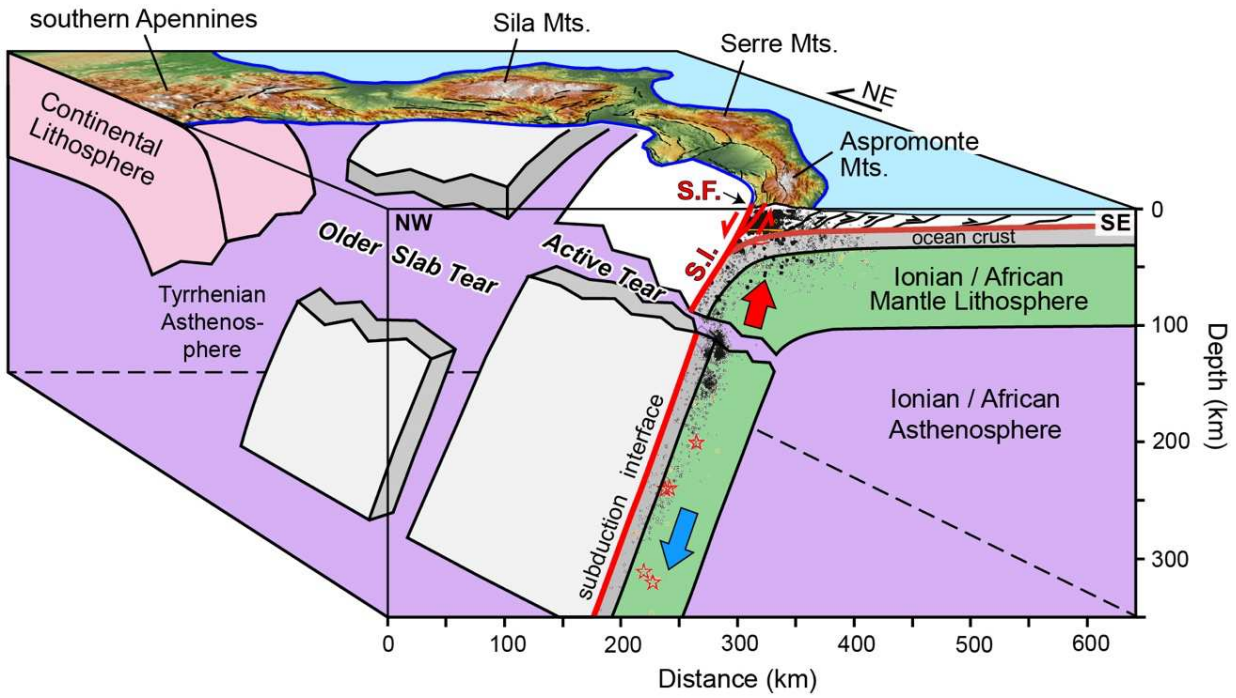


Figure 5. Schematic 3D view of torn slabs beneath southern Italy based on results of this and other studies. Earthquake hypocenters (small circles and red stars) are from ref. 21 (Fig. 12e); upper mantle structure is adapted from seismic, gravity, and tomographic studies (refs. 16-19). Seismic data reveal a kink and discontinuity of hypocenters beneath the Aspromonte Mts. (ref. 21) interpreted here to be a small active tear in the Ionian slab. We infer that rapid uplift represents an ongoing response to slab break-off that geodynamic models predict will last no more than ~0.5 Myr. (e.g., ref. 26). The seismically active Scilla fault (S.F.) projects down-dip to the subduction interface (S.I.), suggesting that the subduction interface fault was recently reactivated with normal-sense displacement to accommodate rapid isostatic rebound of shallow lithosphere (red arrow) while subduction of the deeper slab continues (blue arrow). This process, known as eduction, is documented in other settings where a subduction interface fault is reversed and reactivated as a normal fault when subduction ends, causing isostatic rebound driven by buoyancy of the crust.

241

242 The seismically active Scilla fault (Fig. 1)[27,28] projects down-dip to the subduction
243 interface above 100 km depth (Fig. 5), suggesting that the subduction interface fault was
244 recently reactivated with normal-sense displacement to accommodate rebound of shallow
245 lithosphere. This process, known as "eduction", is simulated in geodynamic models[25,42,43]
246 and documented at other convergent margins where breakoff of a subducting slab cancels
247 the slab pull force, causing rapid buoyancy-driven isostatic rebound and reversal of the
248 subduction interface as a large normal fault[44,45]. Although normal-sense earthquakes have
249 not been recorded on the subduction interface itself, eduction is consistent with seismic
250 evidence for down-dip extension of the shallow slab[20] and b-value anomalies that are
251 commonly associated with slab detachment and fragmentation in other similar settings[22].
252 While this mechanism is often invoked where continental collision leads to stalling of
253 subduction and slab breakoff, the Ionian ocean slab is known to be torn in northern Calabria
254 and NE Sicily due to lateral escape between the converging African and European
255 margins[13,16–18]. Indeed, slab tearing beneath southern Calabria is the expected outcome of
256 migrating tear events that are well documented in nearby adjacent regions (Fig. 1a)[3,13,16–18].
257

258 **Implications for active faulting and seismic hazards**

259 Rates of surface uplift and fault throw documented here (Fig. 4, Table 1) are 5 to 10 times
260 faster than rates calculated in previous studies[7,24,28–30,37]. Many prior estimates were based
261 on a ~1.0-Ma age for the SCA marine terraces above 1,000 masl[34,35], but this age was recently
262 shown to be unreliable because the terraces are younger than 0.48 Ma[38]. Recent advances
263 in luminescence dating (see Methods) allow us to quantify the age of previously undated
264 terraces above 200 masl, providing new insight into the rates and geodynamic drivers of
265 active faulting in southern Calabria. This result also raises numerous new questions. For
266 example, fault-throw rates averaged over the last ~120 kyr (Table 1) lack the temporal
267 resolution needed to discern shorter-term variations. Meschis et al. (ref. [31]) proposed a
268 model for fault interactions in which throw rate on the Messina-Taormina fault increased at
269 ~50 ka while rates decreased on the Reggio Calabria and Armo faults, marking a structural

reorganization during constant-rate regional extension. This hypothesis warrants further testing with new mapping and terrace dating. Similarly, lower slip rates previously reported for the Cittanova fault[46,47] differ from slip rates implied by our results (Table 1). Reconciling this discrepancy will require future work to integrate independent age constraints.

The results of this study are important for assessment of geohazards in southern Calabria and northeast Sicily, one of the highest seismic risk areas in the Mediterranean region[20,21,27,32]. Long-term slip rate is a fundamental parameter used in probabilistic seismic hazard analysis to calculate strain accumulation and earthquake recurrence on active faults[48], and it is a key constraint in numerical models and comparative analyses that explore how fault system geometry, fault interactions, triggering, and stress transfer influence historical earthquakes in Italy[49,50]. A short recurrence time of 125–150 years documented from macroseismic analysis[32], compared to prior estimates of ca. 1,400–4,400 years based on paleoseismic studies[46,47], could reflect either long-term strain accumulation or an ongoing temporal cluster of earthquakes. Because fault displacements in this region occur as footwall uplift with little or no hanging-wall subsidence (a pattern consistent with active isostatic rebound), the total dip-slip offset accrued over multiple earthquakes can be compared to uplift rates for elevations >1,000 masl which capture total slip on major faults in the study area. Three seismic cycles documented north of the Coccorino fault (Fig. 1b) produced a total of 3–5 m fault throw (roughly equal to true slip for steep faults in the study area[27,28]) over 400 years[32], for a time-averaged slip rate of ~7.5–12.5 mm yr^{-1}. Because the first cycle is not recorded farther south (Cittanova, Sant'Eufemia, Scilla faults), rates in that area are assessed for cycles 2 and 3 which produced ~2.0–2.5 m of offset during the period 1750 to 2000 CE (250 yr)[32], for a summed rate of 8–10 mm yr^{-1}. These values broadly overlap calculated uplift rates of 8–12 mm yr^{-1} averaged over 119 kyr for high-elevation terraces in this study (Fig. 4), though the short historical window and unclear fraction of slip released during earthquakes suggest this agreement is a first-order consistency check rather than independent confirmation.

In summary, we have used luminescence dating methods to document rates of uplift (<1 to >12 mm yr^{-1}) and fault throw (0.8 to 4.2 mm yr^{-1}) in southern Calabria that are 5–10

times faster than previously published estimates. Our results support a hypothesis for active tearing of the Ionian slab that has been debated for more than 30 years. Slab breakoff and isostatic rebound are widely invoked to explain the geologic evolution of collisional margins, but active slab tearing is rarely captured in-progress due to the short duration of very rapid uplift (<0.5 Myr[26]). These new insights on the transient surface response to strong mantle-surface coupling are generally applicable to other subduction systems, and are important for better understanding seismic hazards in this earthquake-prone region.

Methods

Sample Collection

Samples were collected by hammering 25 cm long, 5 cm diameter opaque steel tubes into fresh exposures of weakly cemented sands following standard methods[51] (Figs. 3b, 3c; Supplementary Figs. 7–12). The ends of the tubes were covered with aluminum foil and taped to prevent light exposure and mixing during transport. Sediments were characterized in the field by description and measurement of lithofacies, grain size, sorting, sedimentary structures, bed thickness, fossil content, burrows, and other features. Depth of each sample below the present land surface (overburden) was also measured.

Sample preparation and measurement details

Luminescence dating samples were prepared under dim, indirect amber lighting conditions at the University of Texas at Arlington Luminescence Laboratory. The outer 3 cm from both ends of sample tubes were removed for gravimetric water content measurement. From these outer ends, 10 g subsamples were sent to SGS Canada for elemental concentration measurement with inductively coupled plasma mass spectrometry (ICP-MS) and optical emission spectroscopy (ICP-OES). The interior portions of tubes were wet sieved to isolate a grain size of 150 – 200 μm. Magnetic minerals were removed, then grains were digested in hydrochloric acid and then hydrogen peroxide for 3 h each, to remove carbonates and organics, respectively. Grains were then floated in lithium metatungstate of density 2.565 g/cm^3 to target the most potassic feldspar minerals[52]. Geologic dose rates were calculated using the DRAC online calculator[53]. We assumed an internal potassium content

of 12.5 ± 0.5 wt.% [54], conversion factors of Liritzis et al. (ref. [55]), and attenuation factors from Guerin et al. (ref. [56]).

All luminescence measurements were done on a Risø DA-20 TL/OSL automated luminescence reader. We used a single aliquot regenerative[57] post-infrared infrared stimulated luminescence protocol[58] modified for single grain dating[59]. Following a natural or regenerative dose, discs were preheated to 250 °C for 10 s to remove thermally unstable signal components. Grains were then individually stimulated with an infrared laser for 3 s each at a hold temperature of 50 °C to measure the IR_{50} signal. Discs were then heated to 225 °C and grains were again stimulated for 3 s each, this time to measure the post-IR $IRSL_{225}$ signal. This signal is less affected by anomalous fading than the lower-temperature signal[60]. A laboratory dose was given and then discs were heated and stimulated at 50 and 225 °C again to measure the test dose response. Finally, discs were heated to 290 °C and stimulated with infrared diodes for 40 s to remove any residual signal. This cycle was repeated for a series of regenerative doses to construct dose response curves for each grain, from which the equivalent dose values of were measured. Equivalent dose values were calculated using the three-parameter minimum dose model[61] assuming an overdispersion of 20%[62].

To quantify anomalous fading for the post-IR $IRSL_{225}$ signal, 2 discs per sample for three samples were given regenerative doses of 153 Gy, preheated, then kept dark at room temperature for durations ranging from 1 h up to 7 d. The weighted mean *g*-value is 0.855 ± 0.135 % loss per decade[63]. This *g*-value was rescaled to a dimensionless *ρ'*-value and then apparent ages were corrected for fading using the approach of Kars et al. (ref. [64]) with uncertainty propagation following Guralnik and King (ref. [65]).

Map Work and Drafting

Digital elevation models (DEMs) and derivative slope maps were extracted from Tinitaly 10-m digital elevation model, available at https://tinitaly.pi.ingv.it/ [66], and manipulated in QGIS for map production. Topographic profiles were generated in QGIS using the Profile Tool Plugin. Ground deformation data were downloaded from the European Ground Motion Service InSAR database (https://egms.land.copernicus.eu/). Images were adjusted in Adobe Photoshop, and final figures were drafted using Adobe Illustrator.

References

1. Braun, J. The many surface expressions of mantle dynamics. *Nat. Geosci.* **3**, 825–833 (2010).

2. Flament, N., Gurnis, M. & Dietmar Müller, R. A review of observations and models of dynamic topography. *Lithosphere* **5**, 189–210 (2013).

3. Faccenna, C. & Becker, T. W. Topographic expressions of mantle dynamics in the Mediterranean. *Earth. Sci. Rev.* **209**, 103327 (2020).

4. Sternai, P. *et al.* Present-day uplift of the European Alps: Evaluating mechanisms and models of their relative contributions. *Earth. Sci. Rev.* **190**, 589–604 (2019).

5. Gallen, S. F., Seymour, N. M., Glotzbach, C., Stockli, D. F. & O'Sullivan, P. Calabrian forearc uplift paced by slab–mantle interactions during subduction retreat. *Nat. Geosci.* **16**, 513–520 (2023).

6. Morel, D. L., Morell, K. D., Keller, E. A. & Rittenour, T. M. Quaternary chronology and rock uplift recorded by marine terraces, Gaviota coast, Santa Barbara County, California, USA. *Bulletin of the Geological Society of America* **134**, 871–884 (2022).

7. Antonioli, F. *et al.* Late Pleistocene to Holocene record of changing uplift rates in southern Calabria and northeastern Sicily (southern Italy, Central Mediterranean Sea). *Tectonophysics* **422**, 23–40 (2006).

8. Robertson, J., Meschis, M., Roberts, G. P., Ganas, A. & Gheorghiu, D. M. Temporally Constant Quaternary Uplift Rates and Their Relationship With Extensional Upper-Plate Faults in South Crete (Greece), Constrained With 36Cl Cosmogenic Exposure Dating. *Tectonics* **38**, 1189–1222 (2019).

9. Rosenbaum, G. & Lister, G. S. Neogene and Quaternary rollback evolution of the Tyrrhenian Sea, the Apennines, and the Sicilian Maghrebides. *Tectonics* **23**, (2004).

10. Royden, L. & Faccenna, C. Subduction Orogeny and the Late Cenozoic Evolution of the Mediterranean Arcs. *Annu. Rev. Earth Planet. Sci.* **46**, 261–289 (2018).

11. Wortel, M. J. R. & Spakman, W. Subduction and Slab Detachment in the Mediterranean-Carpathian Region. *Science (1979).* **290**, 1910–1917 (2000).

12. Spakman, W. & Wortel, R. A Tomographic View on Western Mediterranean Geodynamics. in *The TRANSMED Atlas. The Mediterranean Region from Crust to Mantle* 31–52 (Springer Berlin Heidelberg, Berlin, Heidelberg, 2004). doi:10.1007/978-3-642-18919-7_2.

13. Faccenna, C., Becker, T. W., Miller, M. S., Serpelloni, E. & Willett, S. D. Isostasy, dynamic topography, and the elevation of the Apennines of Italy. *Earth Planet. Sci. Lett.* **407**, 163–174 (2014).

14. Van Der Meulen, M. J., Meulenkamp, J. E. & Wortel, M. J. R. *Lateral Shifts of Apenninic Foredeep Depocentres Reflecting Detachment of Subducted Lithosphere*. *Earth and Planetary Science Letters* vol. 154 (1998).

15. Ascione, A., Ciarcia, S., Di Donato, V., Mazzoli, S. & Vitale, S. The Pliocene-Quaternary wedge-top basins of southern Italy: an expression of propagating lateral slab tear beneath the Apennines. *Basin Research* **24**, 456–474 (2012).

16. Neri, G., Orecchio, B., Totaro, C., Falcone, G. & Presti, D. Subduction beneath southern Italy close the ending: Results from seismic tomography. *Seismological Research Letters* **80**, 63–70 (2009).

17. Faccenna, C. *et al.* Topography of the Calabria subduction zone (southern Italy): Clues for the origin of Mt. Etna. *Tectonics* **30**, (2011).

18. Scarfì, L. *et al.* Slab narrowing in the Central Mediterranean: The Calabro-Ionian subduction zone as imaged by high resolution seismic tomography. *Sci. Rep.* **8**, (2018).

19. Maesano, F. E., Tiberti, M. M. & Basili, R. The Calabrian Arc: three-dimensional modelling of the subduction interface. *Sci. Rep.* **7**, 8887 (2017).

20. Presti, D., Totaro, C., Neri, G. & Orecchio, B. New Earthquake Data in the Calabrian Subduction Zone, Italy, Suggest Revision of the Presumed Dynamics in the Upper Part of the Subducting Slab. *Seismological Research Letters* **90**, 1994–2004 (2019).

21. Latorre, D., Di Stefano, R., Castello, B., Michele, M. & Chiaraluce, L. An updated view of the Italian seismicity from probabilistic location in 3D velocity models: The 1981–2018 Italian catalog of absolute earthquake locations (CLASS). *Tectonophysics* **846**, 229664 (2023).

22. Godano, C., Petrillo, G., Tramelli, A. & Convertito, V. The b b-Value Tomography of the Calabrian Arc. *Earth and Space Science* **12**, 1–7 (2025).

23. Pirrotta, C. *et al.* Recent Activity and Kinematics of the Bounding Faults of the Catanzaro Trough (Central Calabria, Italy): New Morphotectonic, Geodetic and Seismological Data. *Geosciences (Basel).* **11**, 405 (2021).

24. Westaway, R. Quaternary uplift of southern Italy. *J. Geophys. Res.* **98**, 21,741-21,772 (1993).

25. Duretz, T. & Gerya, T. V. Slab detachment during continental collision: Influence of crustal rheology and interaction with lithospheric delamination. *Tectonophysics* **602**, 124–140 (2013).

26. Maiti, G. *et al.* Topography Response to Horizontal Slab Tearing and Oblique Continental Collision: Insights From 3D Thermomechanical Modeling. *J. Geophys. Res. Solid Earth* **129**, (2024).

27. Jacques, E., Monaco, C., Tapponnier, P., Tortorici, L. & Winter, T. Faulting and earthquake triggering during the 1783 Calabria seismic sequence. *Geophys. J. Int.* **147**, 499–516 (2001).

28. Catalano, S., De Guidi, G., Monaco, C., Tortorici, G. & Tortorici, L. Active faulting and seismicity along the Siculo-Calabrian Rift Zone (Southern Italy). *Tectonophysics* **453**, 177–192 (2008).

29. Roda-Boluda, D. C. & Whittaker, A. C. Structural and geomorphological constraints on active normal faulting and landscape evolution in Calabria, Italy. *J. Geol. Soc. London.* **174**, 701–720 (2017).

30. Quye-Sawyer, J., Whittaker, A. C., Roberts, G. G. & Rood, D. H. Fault Throw and Regional Uplift Histories From Drainage Analysis: Evolution of Southern Italy. *Tectonics* **40**, (2021).

31. Meschis, M. *et al.* Out of phase Quaternary uplift-rate changes reveal normal fault interaction, implied by deformed marine palaeoshorelines. *Geomorphology* **416**, 108432 (2022).

32. Andrenacci, C. *et al.* Reappraisal and Analysis of Macroseismic Data for Seismotectonic Purposes: The Strong Earthquakes of Southern Calabria, Italy. *Geosciences (Basel).* **13**, 212 (2023).

33. Dorsey, R. J., Longhitano, S. G. & Chiarella, D. Structure and morphology of an active conjugate relay zone, Messina Strait, southern Italy. *Basin Research* **36**, (2024).

34. Barrier, P., Alo, I. T., Geronimo, D. I. & Lanzafame, G. I rapporti tra tettonica e sedimentazione nell'evoluzione recente dell'Aspromonte Occidentale (Calabria). *Rivista italiana di paleontologia e stratigrafia* **91**, 537–556 (1986).

35. Miyauchi, T., Dai Pra, G. & Sylos Labini, S. Geochronology of Pleistocene marine terraces and regional tectonics in the Tyrrhenian coast of South Calabria. *Il Quaternario* **7**, 17–34 (1994).

36. Balescu, S. *et al.* Thermoluminescence dating tests of Pleistocene sediments from uplifted marine shorelines along the southwest coastline of the Calabrian Peninsula (southern Italy). *Palaeogeogr. Palaeoclimatol. Palaeoecol.* **130**, 25–41 (1997).

37. Antonioli, F. *et al.* New Evidence of MIS 3 Relative Sea Level Changes from the Messina Strait, Calabria (Italy). *Water (Basel).* **13**, 2647 (2021).

38. Dorsey, R. J. *et al.* Revised history of Pleistocene vertical motions in NE Sicily and southern Calabria, Italy, from 40Ar/39Ar dating and fault zone morphology. *Tectonics* **45**, (2026).

39. Cardello, G. L., Barreca, G., Monaco, C., de Michele, M. & Antonioli, F. First comparison of subsidence/uplift rates between Copernicus European Ground Motion Service data and long-term MIS 5.5 geological record in Mediterranean regions. *Earth. Sci. Rev.* **265**, 105132 (2025).

40. Roda-Boluda, D. C., D'Arcy, M., Whittaker, A. C., Gheorghiu, D. M. & Rodés, Á. 10Be erosion rates controlled by transient response to normal faulting through incision and landsliding. *Earth Planet. Sci. Lett.* **507**, 140–153 (2019).

41. Van der Meulen, M. J., Buiter, S. J. H., Meulenkamp, J. E. & Wortel, M. J. R. An early Pliocene uplift of the central Apenninic foredeep and its geodynamic significance. *Tectonics* **19**, 300–313 (2000).

42. Gerya, T. Numerical modeling of subduction: State of the art and future directions. *Geosphere* **18**, 503–561 (2022).

43. Andrić, N. *et al.* Variability of orogenic magmatism during Mediterranean-style continental collisions: A numerical modelling approach. *Gondwana Research* **56**, 119–134 (2018).

44. Brueckner, H. K. & Cuthbert, S. J. Extension, disruption, and translation of an orogenic wedge by exhumation of large ultrahigh-pressure terranes: Examples from the Norwegian Caledonides. *Lithosphere* **5**, 277–289 (2013).

45. Petersen, K. D. & Buck, W. R. Eduction, extension, and exhumation of ultrahigh-pressure rocks in metamorphic core complexes due to subduction initiation. *Geochemistry, Geophysics, Geosystems* **16**, 2564–2581 (2015).

46. Galli, P. A. C. & Peronace, E. Low slip rates and multimillennial return times for M_w 7 earthquake faults in southern Calabria (Italy). *Geophys. Res. Lett.* **42**, 5258–5265 (2015).

47. Galli, P. & Bosi, V. Paleoseismology along the Cittanova fault: Implications for seismotectonics and earthquake recurrence in Calabria (southern Italy). *J. Geophys. Res. Solid Earth* **107**, (2002).

48. Faure Walker, J. P. *et al.* Variable Fault Geometry Suggests Detailed Fault-Slip-Rate Profiles and Geometries Are Needed for Fault-Based Probabilistic Seismic Hazard Assessment (PSHA). *Bulletin of the Seismological Society of America* **109**, 110–123 (2019).

49. Sgambato, C., Faure Walker, J. P., Roberts, G. P., Mildon, Z. K. & Meschis, M. Influence of Fault System Geometry and Slip Rates on the Relative Role of Coseismic and Interseismic Stresses on Earthquake Triggering and Recurrence Variability. *J. Geophys. Res. Solid Earth* **128**, (2023).

50. Meschis, M. *et al.* Empirical Scaling Relationships Between Fault Length and Throw-Rates Modulated by Fault Interactions in Extensional Regimes. *Tectonics* **45**, (2026).

51. Nelson, M. S. *et al.* User Guide for Luminescence Sampling in Archaeological and Geological Contexts. *Advances in Archaeological Practice* **3**, 166–177 (2015).

52. Rhodes, E. J. Dating sediments using potassium feldspar single-grain IRSL: Initial methodological considerations. *Quaternary International* **362**, 14–22 (2015).

53. Durcan, J. A., King, G. E. & Duller, G. A. T. DRAC: Dose Rate and Age Calculator for trapped charge dating. *Quat. Geochronol.* **28**, 54–61 (2015).

54. Huntley, D. J. & Baril, M. R. K content of the K-feldspars being measured in optical dating or in thermoluminescence dating. *Ancient TL* **15**, 11–13 (1997).

55. Liritzis, I., Stamoulis, K. & Ioannides. A re-evaluation of radiation dose-rate conversion factors. *Mediterranean Archaeology and Archaeometry* **13**, 1–15.

56. Guérin, G., Mercier, N., Nathan, R., Adamiec, G. & Lefrais, Y. On the use of the infinite matrix assumption and associated concepts: A critical review. *Radiat. Meas.* **47**, 778–785 (2012).

57. Wintle, A. G. & Murray, A. S. A review of quartz optically stimulated luminescence characteristics and their relevance in single-aliquot regeneration dating protocols. *Radiat. Meas.* **41**, 369–391 (2006).

58. Buylaert, J. P., Murray, A. S., Thomsen, K. J. & Jain, M. Testing the potential of an elevated temperature IRSL signal from K-feldspar. *Radiat. Meas.* **44**, 560–565 (2009).

59. Brown, N. D., Rhodes, E. J., Antinao, J. L. & McDonald, E. V. Single-grain post-IR IRSL signals of K-feldspars from alluvial fan deposits in Baja California Sur, Mexico. *Quaternary International* **362**, 132–138 (2015).

60. Thomsen, K. J., Murray, A. S., Jain, M. & Bøtter-Jensen, L. Laboratory fading rates of various luminescence signals from feldspar-rich sediment extracts. *Radiat. Meas.* **43**, 1474–1486 (2008).

61. Galbraith, R. F., Roberts, R. G., Laslett, G. M., Yoshida, H. & Olley, J. M. Optical dating of single and multiple grains of quartz from Jinmium rock shelter, northern Australia: Part I, experimental design and statistical models. *Archaeometry* **41**, 339–364 (1999).

62. Arnold, L. J. & Roberts, R. G. Stochastic modelling of multi-grain equivalent dose (De) distributions: Implications for OSL dating of sediment mixtures. *Quat. Geochronol.* **4**, 204–230 (2009).

63. Huntley, D. J. & Lamothe, M. Ubiquity of anomalous fading in K-feldspars and the measurement and correction for it in optical dating. *Can. J. Earth Sci.* **38**, 1093–1106 (2001).

64. Kars, R. H., Wallinga, J. & Cohen, K. M. A new approach towards anomalous fading correction for feldspar IRSL dating — tests on samples in field saturation. *Radiat. Meas.* **43**, 786–790 (2008).

65. Guralnik, B. & King, G. E. Anomalous fading correction in luminescence dating – a mathematical reappraisal. Preprint at https://doi.org/10.5194/egusphere-2025-4186 (2025).

66. Tarquini, S., Isola, I., Favalli, M., Battistini, A. & Dotta, G. *TINITALY, a Digital Elevation Model of Italy with a 10 Meters Cell Size (Version 1.1)*. https://tinitaly.pi.ingv.it/ (2023).

Acknowledgements

Funding for this research was provided to R.J.D. by the University of Oregon. Fieldwork expenses were provided to D.C. by Royal Holloway and Sval Energy within the remit of the Fault-controlled deposits Phase 2 research project. M.M. was supported by an INGV-led project (Idro1.RM task 1 9999.710 CR 7101—Rete multiparametrica).

Author Contributions

The research was conceived by R.J.D. Sample collection, curation, and shipping were performed by C.P.O., R.J.D., N.D.B., S.G.L., M.M., and D.C. Samples were analysed by N.D.B. The first draft of the manuscript was written by R.J.D. and N.D.B., with further editing and input from all authors.

Competing Interests

The authors declare no competing interests.

Data availability

Luminescence data are provided in Supplementary Tables 1 and 2, and plots of results are presented in Supplementary Figures 1–4. Additional datasets generated during the current study are available from N.D.B. on reasonable request. Elevation data are available at https://tinitaly.pi.ingv.it/. Ground deformation data were downloaded from the European Ground Motion Service InSAR database (https://egms.land.copernicus.eu/).

Supplementary Files

This is a list of supplementary files associated with this preprint. Click to download.

- SupplementaryFiguresopt300dpi.pdf
- SupplementaryMaterials.pdf
- Table1.docx